

## Research Paper

# $^{64}\text{Cu}$ Labeled Sarcophagine Exendin-4 for MicroPET Imaging of Glucagon like Peptide-I Receptor Expression

Zhanhong Wu<sup>1</sup>, Shuanglong Liu<sup>2</sup>, Indu Nair<sup>1</sup>, Keiko Omori<sup>1</sup>, Stephen Scott<sup>1</sup>, Ivan Todorov<sup>1</sup>, John E. Shively<sup>3</sup>, Peter S. Conti<sup>2</sup>, Zibo Li<sup>2</sup>✉, Fouad Kandeel<sup>1</sup>✉

1. Department of Diabetes and Metabolic Diseases Research, Beckman Research Institute of the City of Hope, Duarte, CA 91010, USA.
2. Molecular Imaging Center, Department of Radiology, University of Southern California, Los Angeles, CA 90033, USA.
3. Department of Immunology, Beckman Research Institute of the City of Hope, Duarte, CA 91010, USA.

✉ Corresponding authors: Fouad Kandeel, M.D., Ph.D. Address: Department of Diabetes and Metabolic Diseases Research, Beckman Research Institute of the City of Hope, 1500 East Duarte Road, Duarte, CA 91010. Phone: (626)301-8282; Fax: (626)301-8489; Email: fkandeel@coh.org. Zibo Li, Ph.D. Address: Department of Radiology, University of Southern California, 2250 Alcazar St, CSC 103, Los Angeles, CA 90033. Phone: (323)442-3252; Fax: (323)442-3253; Email: ziboli@usc.edu

© Ivyspring International Publisher. This is an open-access article distributed under the terms of the Creative Commons License (<http://creativecommons.org/licenses/by-nc-nd/3.0/>). Reproduction is permitted for personal, noncommercial use, provided that the article is in whole, unmodified, and properly cited.

Received: 2013.09.25; Accepted: 2014.04.17; Published: 2014.05.24

## Abstract

The Glucagon-like peptide I receptor (GLP-IR) has become an important target for imaging due to its elevated expression profile in pancreatic islets, insulinoma, and the cardiovascular system. Because native GLP-I is degraded rapidly by dipeptidyl peptidase-IV (DPP-IV), several studies have conjugated different chelators to a more stable analog of GLP-I (such as exendin-4) as PET or SPECT imaging agents with various advantages and disadvantages. Based on the recently developed Sarcophagine chelator, here, we describe the construction of GLP-IR targeted PET probes containing monomeric and dimeric exendin-4 subunit. The *in vitro* binding affinity of BaMalSar-exendin-4 and Mal<sub>2</sub>Sar-(exendin-4)<sub>2</sub> was evaluated in INS-1 cells, which over-express GLP-IR. Mal<sub>2</sub>Sar-(exendin-4)<sub>2</sub> demonstrated around 3 times higher binding affinity compared with BaMalSar-exendin-4. After  $^{64}\text{Cu}$  labeling, microPET imaging of  $^{64}\text{Cu}$ -BaMalSar-exendin-4 and  $^{64}\text{Cu}$ -Mal<sub>2</sub>Sar-(exendin-4)<sub>2</sub> were performed on subcutaneous INS-1 tumors, which were clearly visualized with both probes. The tumor uptake of  $^{64}\text{Cu}$ -Mal<sub>2</sub>Sar-(exendin-4)<sub>2</sub> was significantly higher than that of  $^{64}\text{Cu}$ -BaMaSarI-exendin-4, which could be caused by polyvalency effect. The receptor specificity of these probes was confirmed by effective blocking of the uptake in both tumor and normal positive organs with 20-fold excess of unlabeled exendin-4. In conclusion, sarcophagine cage conjugated exendin-4 demonstrated persistent and specific uptake in INS-1 insulinoma model. Dimerization of exendin-4 could successfully lead to increased tumor uptake *in vivo*. Both  $^{64}\text{Cu}$ -BaMalSar-exendin-4 and  $^{64}\text{Cu}$ -Mal<sub>2</sub>Sar-(exendin-4)<sub>2</sub> hold a great potential for GLP-IR targeted imaging.

Key words: exendin-4 dimer, Sarcophagine, PET,  $^{64}\text{Cu}$ , insulinoma

## Introduction

Derived from endocrine pancreatic beta cells, insulinoma is a tumor of the pancreas, which also secretes insulin. Because surgical resection of the insulinoma remains the standard treatment for this tumor, and the size of the tumor is usually small, localization imaging with computed tomography (CT) or

magnetic resonance imaging (MRI) is usually required [1, 2], but not always successful, again due to the limited size of the lesion. Recently, somatostatin receptor scintigraphy (SRS) has been introduced as a functional method for the detection of insulinoma [3]. However, the relatively low incidence of somatostatin

subtype receptors makes this method only achieve 40–60% sensitivity[4]. In contrast, the Glucagon-like peptide 1 receptor (GLP-1R) is expressed in >90% of insulinomas with a mean density twice that of SSTR2[5]. Clearly, an imaging probe targeting GLP-1R holds the great potential for insulinoma diagnosis.

Since GLP-1R is highly expressed in insulinoma, ligands of GLP-1R could be converted into molecular imaging probes for insulinoma imaging[6,7]. The Glucagon-like peptide 1 (GLP-1) is an incretin peptide released from the intestine in response to nutrient ingestion; its binding to the GLP-1 receptor (GLP-1R) augments glucose-induced insulin secretion from pancreatic  $\beta$ -cells. Although GLP-1 serves as a ligand for GLP-1R, this peptide gets quickly decomposed *in vivo*, which makes it not suitable for imaging applications. As a more robust and high affinity GLP-1R ligand, exendin-4 is a peptide hormone first isolated by Dr. John Eng in 1992[8]. Exendin-4 displays similar biological properties to human GLP-1, with which it shares 53% sequence identity[9]; however, it is metabolically much more stable than GLP-1, which makes it more suitable for imaging probe construction. Previously, exendin analogues have been labeled[10] with  $^{111}\text{In}$ [11-13],  $^{125}\text{I}$ [14],  $^{99\text{m}}\text{Tc}$ [15],  $^{68}\text{Ga}$ [15-17],  $^{64}\text{Cu}$ [18,19], and  $^{18}\text{F}$ [20-23]. The obtained results have demonstrated promising clinical utility of this imaging approach.

Recently, we and others found that dimeric interactions may successfully increase the affinity of ligand-receptor interactions and, thus, significantly improved tumor targeting over the monomeric analogs in many cases[24, 25]. In this study, we constructed two GLP-1R targeted PET probes containing monomeric and dimeric exendin-4 subunit based on the recently developed Sarcophagine chelator[26-29].

The tumor targeting efficacy and *in vivo* kinetics of the exendin-4 dimer was compared with those of the exendin-4 monomer analog.

## Materials and methods

All commercially available chemical reagents were purchased from Aldrich (St. Louis, MO) and used without further purification. Cys<sup>40</sup>-exendin-4 was purchased from C S Bio Co. (Menlo Park, CA).  $^{64}\text{CuCl}_2$  was obtained from University of Wisconsin (Madison, WI).  $^{125}\text{I}$ -exendin(9-39) was purchased from Perkin Elmer (Wellesley, MA). A typical linear gradient HPLC was used for purification and quality control as following. The reversed-phase HPLC using a Phenomenex® Gemini C18 (Torrance, CA) was performed on a Waters system with model 105S single-channel radiation detector (Carroll & Ramsey Associates). At a flow rate of 1 mL/min, the mobile phase was maintained at 95% solvent A [0.1% trifluoroacetic acid (TFA) in water] and 5% B [0.1% TFA in acetonitrile (MeCN)] from 0–2 min and was changed to 35% solvent A and 65% solvent B through 2–32 min. The UV absorbance was monitored at 218 nm.

### Preparation of BaMalSar-exendin-4

BaMalSar was prepared as previously reported[28], which is available at KeraFAST, Inc[28]. Cys<sup>40</sup>-exendin-4 (2.2 mg 0.5  $\mu\text{mol}$ ) was added to pH 7.0 phosphate buffer containing 0.4 mg BaMalSar (0.6  $\mu\text{mol}$ ) (Fig. 1A). The solution was stirred at room temperature for 1 h and the product was purified by HPLC (Rt: 22.23 min). The product was characterized by LTQ FT mass spectrometry (Thermo, Waltham, MA) (BaMalSar-exendin-4:  $m/z$  4992.52 for  $[\text{MH}]^+$ ,  $\text{C}_{223}\text{H}_{338}\text{N}_{60}\text{O}_{67}\text{S}_2$ , calculated  $[\text{MH}]^+$ : 4992.43).

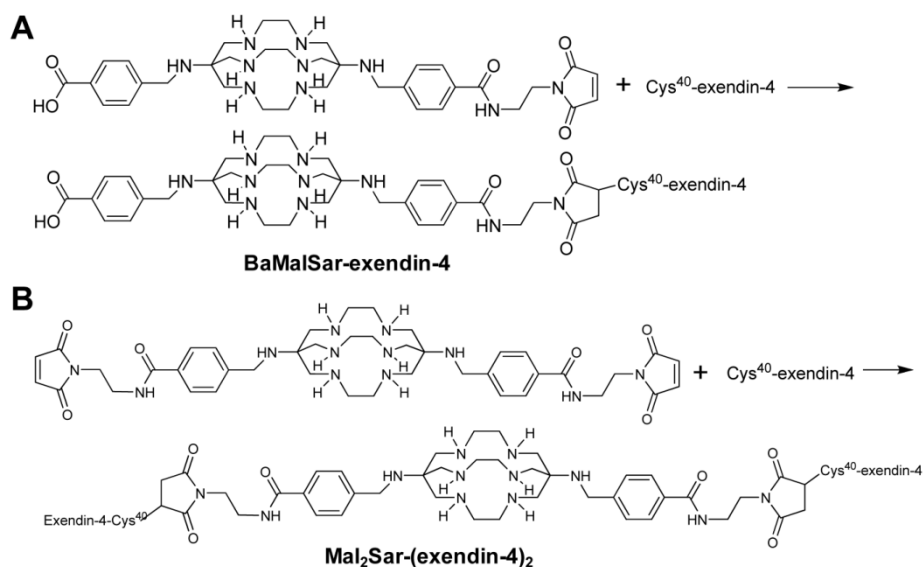


**Figure 1.** Synthesis scheme of monomeric and dimeric exendin-4 analogs: (A) BaMalSar-exendin-4 and (B) Mal<sub>2</sub>Sar-(exendin-4)<sub>2</sub>.

### Preparation of Mal<sub>2</sub>Sar-(exendin-4)<sub>2</sub>

Mal<sub>2</sub>Sar was prepared as previously reported[28]. Cys<sup>40</sup>-exendin-4 (3.3 mg, 0.8 μmol) was added to phosphate buffer (pH 7.0) containing Mal<sub>2</sub>Sar (0.3 mg, 0.36 μmol) (Fig. 1B). The solution was stirred at room temperature and the product was purified by HPLC (Rt: 13.08 min). At a flow rate of 1 mL/min, the mobile phase was maintained at 70% solvent A [0.1% TFA in water] and 30% B [0.1% TFA in MeCN] from 0–2 min and was changed to 35% solvent A and 65% solvent B through 2–37 min. The product was characterized by LTQ FT mass spectrometry (Thermo, Waltham, MA) (Mal<sub>2</sub>Sar-(exendin-4)<sub>2</sub>: m/z 9402.64 for [MH]<sup>+</sup>, C<sub>416</sub>H<sub>630</sub>N<sub>112</sub>O<sub>130</sub>S<sub>4</sub>, calculated[MH]<sup>+</sup>: 9402.50).

### Radiolabeling

BaMalSar-exendin-4 and Mal<sub>2</sub>Sar-(exendin-4)<sub>2</sub> (10 μg) were incubated with 74 MBq of <sup>64</sup>Cu<sup>2+</sup> in 0.1 M sodium acetate buffer (pH 5.5) for 30 min at 37°C. <sup>64</sup>Cu-labeled peptide was subsequently purified by analytical HPLC and the radioactive peak containing the desired product was collected. After removal of the solvent by rotary evaporation, the conjugated peptide tracer was reconstituted in 1 mL phosphate buffer saline (PBS, 1x, Mediatech, Manassas, VA) and passed through a 0.22 μm syringe filter for *in vivo* animal experiments. The decay-corrected radiochemical yield (RCY) for <sup>64</sup>Cu-BaMalSar-exendin-4 and <sup>64</sup>Cu-Mal<sub>2</sub>Sar-(exendin-4)<sub>2</sub> was more than 90%.

### Octanol–water partition coefficient

To determine the lipophilicity of <sup>64</sup>Cu-BaMalSar-exendin-4 and <sup>64</sup>Cu-Mal<sub>2</sub>Sar-(exendin-4)<sub>2</sub>, the final products were diluted in 500 μL PBS (1X) and an equal volume of octanol was added. After mixing vigorously for 10 min, the mixture was separated by centrifugation (5 min; 5000 rpm). Counts in aliquots (n=3) of the organic and inorganic layers were determined using a gamma counter (Packard). The log P values were reported as an average plus the standard deviation[23].

### Cell culture

Rat insulinoma cell line INS-1 (GLP-1R positive, kindly donated by Dr. Ian Sweet, University of Washington, Seattle, WA) was maintained under standard conditions[18]: the INS-1 cells were grown in RPMI-1640 medium supplemented with 10% fetal bovine serum (Atlanta Laboratories, Atlanta, GA), 20mM Hepes, 2mM L-glutamine, 1mM Sodium-pyruvate, 2 mM L-Glutamine, 1 % antibiotic-antimycotic solution (Mediatech, Manassas, VA), and 50 mM 2-mercaptoethanol at 37 °C in humidified atmosphere containing 5% CO<sub>2</sub>. The INS-1 cells were

grown in culture until sufficient cells were available.

### *In vitro* cell binding assay

The *in vitro* GLP-1R-binding affinity and specificity of BaMalSar-exendin-4, Mal<sub>2</sub>Sar-(exendin-4)<sub>2</sub> and exendin-4 were assessed via competitive cell binding assays using <sup>125</sup>I-exendin(9-39) (PerkinElmer, Waltham, MA) as the GLP-1R specific radioligand based on reported procedure[18]. In detail, INS-1 cells were harvested, washed three times with PBS, and resuspended (2 × 10<sup>6</sup> cells/mL) in the binding buffer[30]. Filter multiscreen DV plates (96-well, pore size, 0.65 μm, Millipore, Billerica, MA) were seeded with 10<sup>5</sup> cells and incubated with <sup>125</sup>I-exendin(9-39) (0.74 kBq/well) in the presence of increasing concentrations of different exendin-4 analogues (0–1.0 μmol/L). The truncated exendin(9-39) is an antagonist of GLP-1R and a competitive inhibitor of exendin-4. The total incubation volume was adjusted to 200 μL. After the cells were incubated for 2 h at room temperature, the plates were filtered through a multiscreen vacuum manifold and washed three times with binding buffer. The hydrophilic polyvinylidenedifluoride (PVDF) filters were collected, and the radioactivity was determined using a gamma counter. The best-fit 50% inhibitory concentration (IC<sub>50</sub>) values for INS-1 cells were calculated by fitting the data with nonlinear regression using GraphPad Prism (GraphPad Software, La Jolla, CA). Experiments were performed on triplicate samples.

### Animal model

Male, NOD/SCID mice (the City of Hope Animal Resource Center, Duarte, CA), 8–10 weeks old, served as recipients for insulinoma cells. All animal experiments were performed in compliance with the Guidelines for the Care and Use of Research Animals established by the City of Hope/Beckman Research Institute's Animal Use Committee.

*Xenograft tumor model.* NOD/SCID mice were injected with INS-1 rat insulinoma cells (5 × 10<sup>6</sup>, suspended in 0.1 ml of 1x phosphate buffered saline) subcutaneously in the thigh[18]. Tumors were established within 18–21 days post-injection. Blood glucose values were monitored daily and 6% glucose solution was fed ad libitum once the blood glucose level was lower than 3.3 mmol/L.

### Western blot

Cultured INS-1 cells, INS-1 tumors and organs (liver, pancreas and kidney) harvested from NOD/SCID mice were washed twice with ice cold PBS, flash frozen in a dry ice methanol bath and stored at -80 °C until use. Frozen stored cells and minced tissues were lysed with lysis buffer. Whole cell lysates containing equivalent amount of protein

were separated by SDS-PAGE and western blot was performed as described previously[31]. Rabbit polyclonal antibodies directed against GLP-1R (Abcam, San Francisco, CA) and  $\beta$  actin (Cell Signaling Technology, Danvers, MA) were used at 1:1000 dilution. Densitometric analysis of immunoblots was performed with the NIH image software (ImageJ).

### microPET imaging

microPET imaging of  $^{64}\text{Cu}$ -BaMalSar-exendin-4 and  $^{64}\text{Cu}$ -Mal<sub>2</sub>Sar-(exendin-4)<sub>2</sub> were performed in mice bearing INS-1 tumor to evaluate the *in vivo* specific binding to GLP-1R (n=3). For blocking studies, exendin-4 (20  $\mu\text{g}$ ) was co-injected with the radiotracers. For microPET imaging, mice were injected via the tail vein with 3.7-7.4 MBq of  $^{64}\text{Cu}$ -BaMalSar-exendin-4 or  $^{64}\text{Cu}$ -Mal<sub>2</sub>Sar-(exendin-4)<sub>2</sub>. Serial imaging of INS-1 tumor (at 1, 4 and 24 h; scan duration 10, 10 and 30 min, respectively) was performed using a microPET R4 scanner (Concorde Microsystems, Knoxville, TN; 8 cm axial field of view, spatial resolution 2.0 mm) using previously reported procedures[18]. Images were reconstructed by use of a 2-dimensional ordered-subsets expectation maximization (OSEM) algorithm using the microPET Manager Software (Concorde Microsystems, Knoxville, TN). No background correction was performed. Regions of interest (ROI) were drawn over the tumor on decay-corrected whole-body coronal images. The maximum counts per pixel per minute were obtained from the ROI and converted to counts per milliliter per minute by using a calibration constant. With the assumption of a tissue density of 1 g/ml, the ROIs were converted to counts per gram per min. Image ROI-derived %ID/g values were determined by dividing counts per gram per minute by injected dose. Images were then analyzed using the Acquisition Sinogram Image Processing (ASIPro) software (Concorde Microsystems, Knoxville, TN).

### Histology study

Xenograft INS-1 tumors were collected and fixed with 10% formalin for paraffin embedding. 5- $\mu\text{m}$  parallel sections were stained with hematoxylin and eosin or immunostained for insulin and GLP-1R, as described previously[7, 32]. Guinea pig anti-human insulin (DAKO, Carpinteria, CA) and rabbit anti-human GLP-1R (Novus Biologicals, Littleton, CO) were used as primary antibodies. The corresponding secondary antibodies were conjugated with FITC or Texas Red (Jackson ImmunoResearch, West Grove, PA). The slices were counter-stained for DNA with diamidino-phenylindole (DAPI) (Sigma, St. Louis, MO) and visualized with an Olympus BX51 fluorescent microscope equipped with a Pixera 600 camera.

### Statistical analysis

Quantitative data were expressed as mean  $\pm$  SD. Means were compared using one-way ANOVA and Student's t test. *P* values <0.05 were considered statistically significant.

## Results

### Chemistry and radiochemistry

BaMalSar and Mal<sub>2</sub>Sar were conjugated with Cys<sup>40</sup>-exendin-4 to give BaMalSar-exendin-4 and Mal<sub>2</sub>Sar-(exendin-4)<sub>2</sub> in 90% yields, respectively (Fig. 1). The products were purified by HPLC and characterized by mass spectrometry. The purity of each exendin-4 conjugate was determined to be > 95% by HPLC. The  $^{64}\text{Cu}$  labeling procedure was done within 1 h (including radiolabeling, HPLC purification, solvent evaporation, and reconstruction in PBS) with a decay-corrected yield higher than 90% and more than 98% radiochemical purity. The specific activity of purified  $^{64}\text{Cu}$ -BaMalSar-exendin-4 and  $^{64}\text{Cu}$ -Mal<sub>2</sub>Sar-(exendin-4)<sub>2</sub> were estimated to be 33 GBq/ $\mu\text{mol}$  and 67 GBq/ $\mu\text{mol}$ , respectively. The log *P* values for  $^{64}\text{Cu}$ -BaMalSar-exendin-4 and  $^{64}\text{Cu}$ -Mal<sub>2</sub>Sar-(exendin-4)<sub>2</sub> were determined to be  $-2.33 \pm 0.08$  and  $-2.06 \pm 0.09$ .

### In vitro cell binding assay

We compared the receptor-binding affinity of BaMalSar-exendin-4 and Mal<sub>2</sub>Sar-(exendin-4)<sub>2</sub> with that of exendin-4 using a competitive cell-binding assay (Fig. 2A). Both peptides inhibited the binding of <sup>125</sup>I-exendin(9-39) to GLP-1R positive INS-1 cells in a dose-dependent manner. The IC<sub>50</sub> values for Mal<sub>2</sub>Sar-(exendin-4)<sub>2</sub>, BaMalSar-exendin-4, and exendin-4 were determined to be  $173.1 \pm 79.0$  pmol/L,  $500.0 \pm 134.6$  pmol/L and  $303.3 \pm 1.7$  pmol/L. The results demonstrated that sarcophagine cage conjugation had a minimal effect on the receptor-binding affinity for exendin-4. Mal<sub>2</sub>Sar-(exendin-4)<sub>2</sub> has higher binding affinity than BaMalSar-exendin-4 *in vitro*, which could be caused by polyvalency effect.

### Western blot

The western blot result demonstrated that the liver and kidney has very low GLP-1R expression in NOD/SCID mice and insulinoma (INS-1) has high GLP-1R expression, which is similar with the previous report[6]. Pancreas also has high GLP-1R expression, which makes GLP-1R as an attractive target for non-invasive imaging islets.

### microPET imaging

Static microPET scans were performed on a INS-1 tumor model and representative decay-corrected coronal images at 1, 4 and 24 h after tail vein injection of  $^{64}\text{Cu}$ -BaMalSar-exendin-4 and

$^{64}\text{Cu-Mal}_2\text{Sar-(exendin-4)}_2$  are shown in Fig. 3 and 4, respectively. The INS-1 tumors were clearly visualized with good tumor-to-background contrast for both tracers. The uptake in the tumor or other organs was measured from the ROI analysis and shown in Fig. 5. For  $^{64}\text{Cu-BaMalSar-exendin-4}$ , the tumor uptake was  $11.16 \pm 2.71$ ,  $11.41 \pm 2.91$ , and  $8.07 \pm 2.74$  %ID/g at 1, 4 and 24 h p.i., respectively. For  $^{64}\text{Cu-Mal}_2\text{Sar-(exendin-4)}_2$ , the tumor uptake was  $21.03 \pm 5.06$ ,  $23.29 \pm 5.35$  and  $22.92 \pm 5.64$  %ID/g at 1, 4, and 24 h p.i., respectively. The tumor uptake of  $^{64}\text{Cu-Mal}_2\text{Sar-(exendin-4)}_2$  was significantly higher than that of  $^{64}\text{Cu-BaMalSar-exendin-4}$  ( $P < 0.05$ , Fig. 5) at all time points examined. Both tracers cleared rapidly from the blood, and demonstrated high kidney uptake. The liver uptakes of  $^{64}\text{Cu-BaMalSar-exendin-4}$  and  $^{64}\text{Cu-Mal}_2\text{Sar-(exendin-4)}_2$  were significantly lower than tumor and kidneys at all time-points. The liver uptake of  $^{64}\text{Cu-Mal}_2\text{Sar-(exendin-4)}_2$  ( $6.07 \pm 0.72$ ,  $7.17 \pm 0.58$  and  $7.89 \pm 0.78$  %ID/g at 1, 4 h and 24 h p.i., respectively) was significantly higher than that of  $^{64}\text{Cu-BaMalSar-exendin-4}$  ( $2.51 \pm 0.46$ ,  $3.07 \pm 0.79$  and  $3.02 \pm 0.91$  %ID/g at 1, 4 h and 24 h p.i., respectively), which could be attributed to the larger size of  $\text{Mal}_2\text{Sar-(exendin-4)}_2$ . The nonspecific uptake in the muscle and lung was very low for both tracers.

The GLP-1 targeting specificities of  $^{64}\text{Cu-BaMalSar-exendin-4}$  and  $^{64}\text{Cu-Mal}_2\text{Sar-(exendin-4)}_2$  were demonstrated by blocking studies (Fig. 3 and 4). Co-injection of excess amount of exendin-4 significantly lowered the tumor uptake for  $^{64}\text{Cu-BaMalSar-exendin-4}$  and  $^{64}\text{Cu-Mal}_2\text{Sar-(exendin-4)}_2$ . For example, at 1 h p.i., the tumor uptake of  $^{64}\text{Cu-BaMalSar-exendin-4}$  with blocking dose of exendin-4 agent is 1.41 %ID/g (vs. 11.16 %ID/g without exendin-4). The tumor uptake of  $^{64}\text{Cu-Mal}_2\text{Sar-(exendin-4)}_2$  is 1.49 %ID/g with the blocking exendin-4 agent (vs. 23.29 %ID/g without exendin-4).

### Histology study

Insulinoma is the most common functional pancreatic neuroendocrine neoplasms and is derived from beta cells and secretes insulin. GLP-1R and insulin double staining (Fig. 6) confirmed that the INS-1 tumor has high GLP-1R expression and the tumor uptake was due to GLP-1R targeting effect.

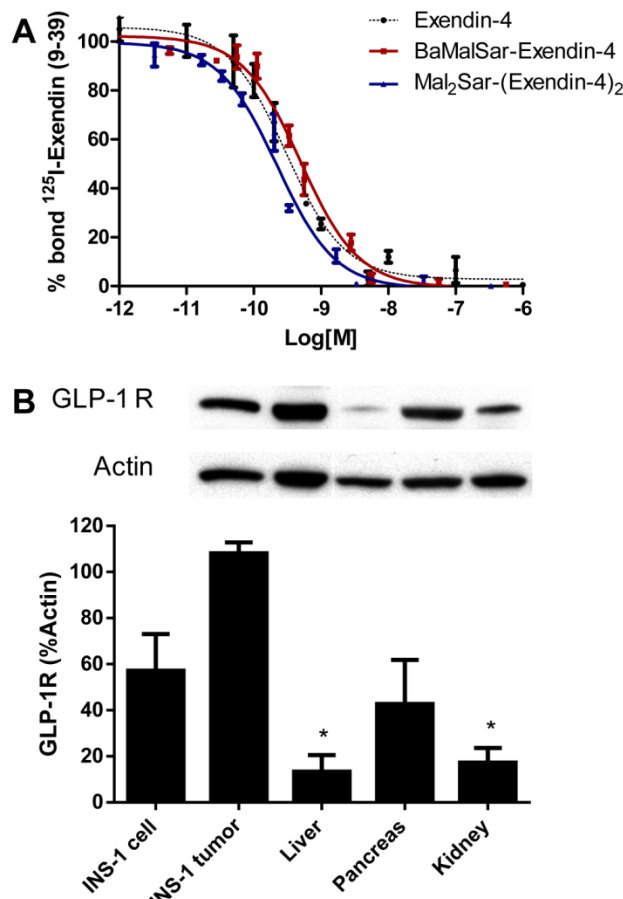


**Figure 2.** (A) Inhibition of  $^{125}\text{I}$ -exendin(9-39) binding to GLP-1R on INS-1 cells by BaMalSar-exendin-4, Mal<sub>2</sub>Sar-(exendin-4)<sub>2</sub> and Exendin-4. Data are mean  $\pm$  SE (n = 3). (B) Western blot analysis of GLP-1R expression in INS cells, INS-1 tumor tissue and major organs. Data is shown as mean  $\pm$  SE (n=3), \* p<0.001 vs. Tumor.

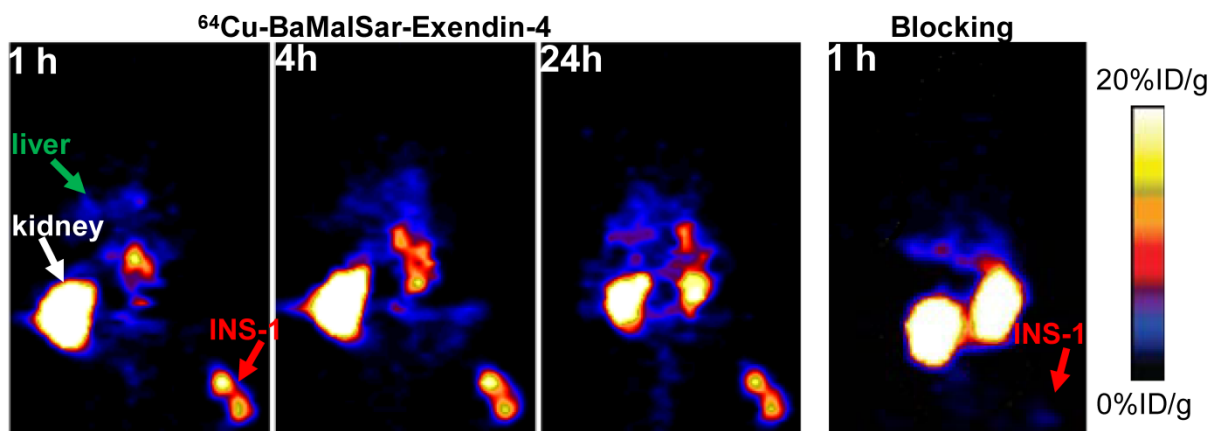


**Figure 3.** Small-animal PET studies of INS-1 tumor-bearing mice. Decay-corrected whole-body coronal images of NOD/SCID mice bearing INS-1 tumor at 1, 4 and 24 h after injection of  $^{64}\text{Cu-BaMalSar-exendin-4}$  without (control, left) and with unradiolabeled exendin-4 (blocking, right).

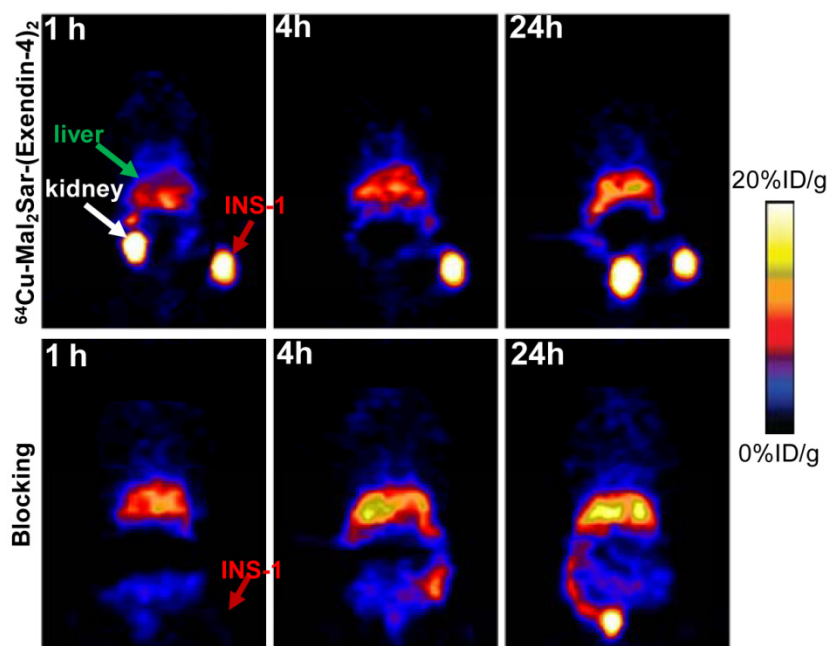


**Figure 4.** Small-animal PET studies of INS-1 tumor-bearing mice. Decay-corrected whole-body coronal images of NOD/SCID mice bearing INS-1 tumor at 1, 4 and 24 h after injection of  $^{64}\text{Cu-Mal}_2\text{Sar-(exendin-4)}_2$  without (control, upper panel) and with unradiolabeled exendin-4 (blocking, lower panel).

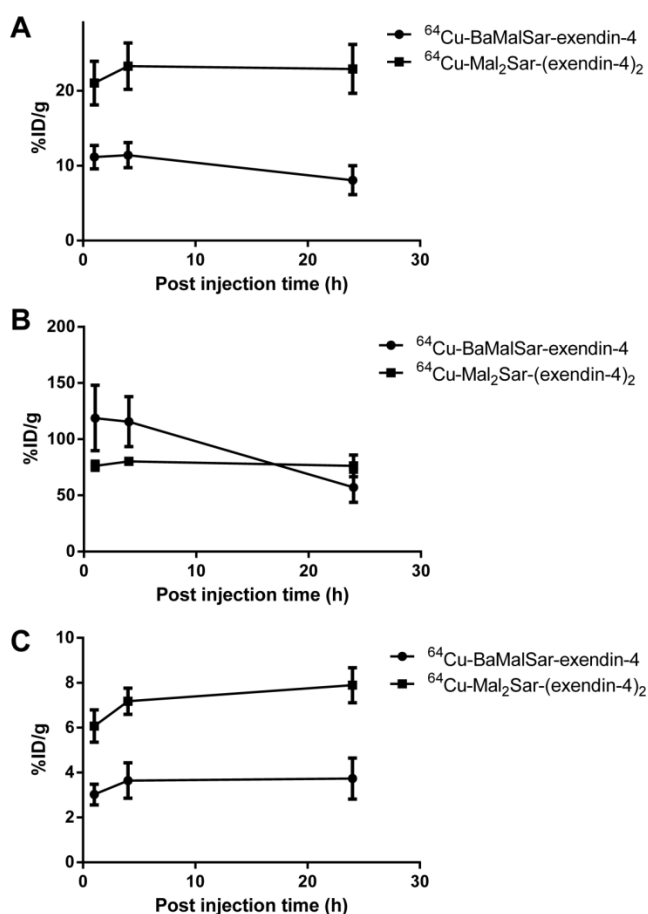


**Figure 5.** Quantitative analyses of small-animal PET data. Time activity curves (TACs) of  $^{64}\text{Cu-BaMalSar-exendin-4}$  and  $^{64}\text{Cu-Mal}_2\text{Sar-(exendin-4)}_2$  on (A) tumor, (B) kidney, and (C) liver.

## Discussion

The Glucagon-like peptide 1 receptor (GLP-1R) has become an important target for imaging due to its elevated expression profile in pancreatic islets, insulinoma, and the cardiovascular system. Because native GLP-1 is degraded rapidly by dipeptidyl peptidase-IV (DPP-IV), several studies have conjugated different chelators to a more stable agonist of GLP-1 (such as exendin-4) as PET or SPECT imaging agents with various advantages and disadvantages. Although various monomeric exendin-4 derivatives have been radiolabeled for imaging applications[10-23], the recent development of dimeric exendin-4 clearly demonstrated the feasibility to improve GLP-1R binding affinity using polyvalency concept[33]. In this study, we constructed  $^{64}\text{Cu}$  labeled monomeric and dimeric exendin-4 as two GLP-1R targeted PET probes based on the recently developed sarcophagine chelator.

With a half-life of 12.7h,  $^{64}\text{Cu}$  is well suited for the radiolabeling of peptides, proteins, and antibodies[34]. Recently, it has been demonstrated that sarcophagine  $^{64}\text{Cu}^{2+}$  complexes are superior to other chelators such as DOTA with respect to *in vivo* stability[26, 27, 35]. The sarcophagine cage has two reactive sites on either end of its cage, which make it an efficient platform for constructing multimeric imaging probes. Recently, we have developed two thio-reactive sarcophagine chelators named BaMalSar and Mal<sub>2</sub>Sar[28]. As shown in Fig. 1, monomeric and dimeric exendin-4 could be successfully synthesized through thiol-maleimide reaction based on these che-

lators. To evaluate the effect of polyvalency, *in vitro* cell binding assay was performed using INS-1 cell (high GLP-1R expression). As expected, Mal<sub>2</sub>Sar-(exendin-4)<sub>2</sub> demonstrated 3 fold increase in receptor binding affinity compared with BaMalSar-exendin-4 due to polyvalency effect. Furthermore, *in vivo* microPET imaging showed that the tumor targeting efficacy of <sup>64</sup>Cu-Mal<sub>2</sub>Sar-(exendin-4)<sub>2</sub> was greater than that of <sup>64</sup>Cu-BaMalSar-exendin-4. Both <sup>64</sup>Cu-Mal<sub>2</sub>Sar-(exendin-4)<sub>2</sub> and <sup>64</sup>Cu-BaMalSar-exendin-4 have relatively low cell uptake (Supplementary Material: Fig. S1). <sup>64</sup>Cu-Mal<sub>2</sub>Sar-(exendin-4)<sub>2</sub> showed slightly slower blood clearance than <sup>64</sup>Cu-BaMalSar-exendin-4 (Supplementary Material: Fig. S2). <sup>64</sup>Cu-Mal<sub>2</sub>Sar-(exendin-4)<sub>2</sub> and <sup>64</sup>Cu-BaMalSar-exendin-4 have similar metabolic stability (Supplementary Material: Fig. S3). The larger molecular size of <sup>64</sup>Cu-Mal<sub>2</sub>Sar-(exendin-4)<sub>2</sub>, along with the stronger target binding affinity, may be attributed to its higher tumor uptake, compared with that of <sup>64</sup>Cu-BaMalSar-exendin-4.

The receptor specificity was successfully demonstrated by blocking experiment. In the presence of cold exendin-4, tumor uptakes of both monomer and dimer were significantly reduced. <sup>64</sup>Cu-Mal<sub>2</sub>Sar-(exendin-4)<sub>2</sub> has much higher liver uptake compared with <sup>64</sup>Cu-BaMalSar-exendin-4, which may be due to the increased molecular weight instead of GLP-1R targeting effect. The western blot result (Fig. 2) demonstrated that liver has very low GLP-1R expression, indicating the liver uptake was not GLP-1R mediated.

Similar to other radiometal labeled exendin-4[10-13,15-17], high and persistent kidney uptake was observed for both <sup>64</sup>Cu-Mal<sub>2</sub>Sar-(exendin-4)<sub>2</sub> and <sup>64</sup>Cu-BaMalSar-exendin-4. Due to low GLP-1R expression in kidney, renal uptake could not be blocked

by excess amount of non-radiolabeled exendin-4. For both imaging and therapeutic applications, it is important to have high tumor-to-kidney ratios, as well as high absolute tumor uptake and persistent tumor retention. For imaging purposes, detection sensitivity around the kidney area will be reduced due to spill over signal from renal area. For therapeutic application, prominent renal uptake would limit the maximum tolerated doses that can be administered due to radiation exposure[36]. Thus, further modification is needed to improve the pharmacokinetics of these <sup>64</sup>Cu labeled exendin-4 radiopharmaceuticals. By inserting a bifunctional linker (such as PEG[37]) between the sarcophagin chelator and the exendin multimer as a pharmacokinetic modifier, we may be able to modulate the overall blood circulation half-life, hydrophilicity, and molecular charges of the radioconjugates, which may possibly improve *in vivo* pharmacokinetics without compromising the tumor-targeting capability. A peptide linker that could be specifically cleaved by kidney would also be considered in our future research[38]. Since <sup>111</sup>In labeled exendin analogue has been used in clinical trial, the radiation exposure caused by <sup>64</sup>Cu should be manageable. The kidneys will be the major organ responsible for dose-limiting toxicity according to our preliminary data. It has been shown, however, that the kidney uptake of radiometal-labeled exendin-4 can be significantly reduced by the administration of a plasma expander such as Gelofusine and PGA[15, 39] without an additive effect on GLP-1R targeting of radiolabeled exendin-4. Nonetheless, an imaging probe with lower kidney accumulation is preferred. Although we used a stable Cu chelator for GLP-1R targeted imaging, the exendin-4 peptide motif has limited stability *in vivo*. Other peptide analogs with increased stability might worth exploring further.

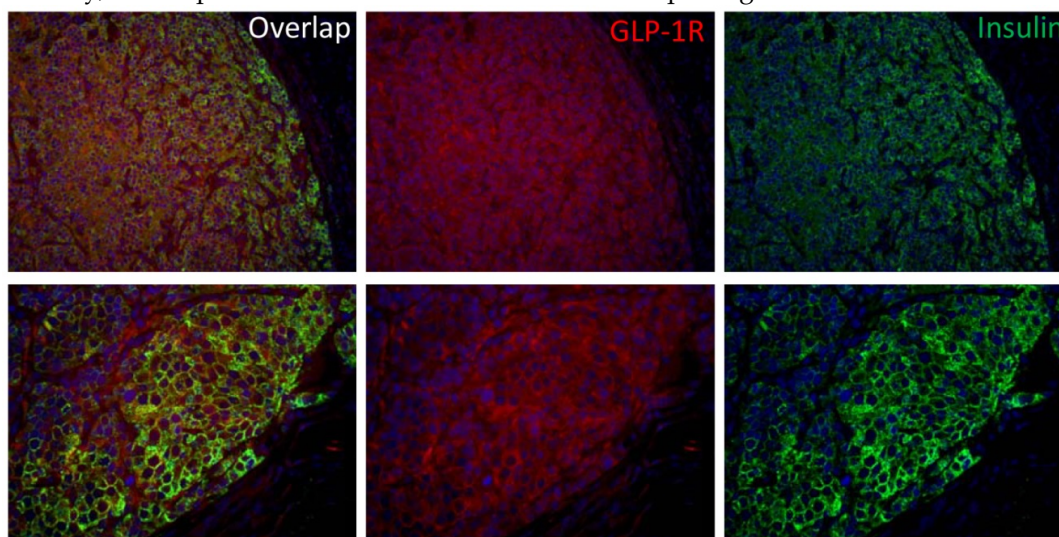


**Figure 6.** Immunofluorescence staining of GLP-1R expression in INS-1 tumor tissue. INS-1 tumor was stained with hematoxylin/eosin (blue), insulin (green) and GLP-1R (red) (top panel: 20X; bottom panel: 40X).

## Conclusions

Sarcophagine cage conjugated exendin-4 demonstrated persistent and specific uptake in INS-1 insulinoma model. Dimerization of exendin-4 could successfully lead to increased tumor uptake *in vivo*. With high kidney radioactivity levels, both  $^{64}\text{Cu}$ -BaMalSar-exendin-4 and  $^{64}\text{Cu}$ -Mal<sub>2</sub>Sar-(exendin-4)<sub>2</sub> may need further optimization before clinical translation.

## Supplementary Material

Figs. S1 - S3. <http://www.thno.org/v04p0770s1.pdf>

## Acknowledgment

This work was supported by the grant from the Juvenile Diabetes Research Foundation International (JDRF-37-2009-20), Jonas Bros Foundation, the American Cancer Society (121991-MRSG-12-034-01-CCE), and the USC Department of Radiology.

## Competing Interests

The authors have declared that no competing interest exists.

## References

- Noone TC, Hoseney J, Firat Z, Semelka RC. Imaging and localization of islet-cell tumours of the pancreas on CT and MRI. *Best Pract. Res Clin Endocrinol Metab.* 2005; 19: 195-211.
- Thoeni RF, Mueller-Lisse UG, Chan R, Do NK, Shyn PB. Detection of small, functional islet cell tumors in the pancreas: selection of MR imaging sequences for optimal sensitivity. *Radiology.* 2000; 214: 483-90.
- Schillaci O, Massa R, Scopinaro F.  $^{111}\text{In}$ -pentetreotide scintigraphy in the detection of insulinomas: importance of SPECT imaging. *J Nucl Med.* 2000; 41: 459-62.
- Bertherat J, Tenenbaum F, Perlemonne K, Videau C, Alberini JL, Richard B, et al. Somatostatin receptors 2 and 5 are the major somatostatin receptors in insulinomas: an *in vivo* and *in vitro* study. *J Clin Endocrinol Metab.* 2003; 88: 5353-60.
- Reubi JC, Waser B. Concomitant expression of several peptide receptors in neuroendocrine tumours: molecular basis for *in vivo* multireceptor tumour targeting. *Eur J Nucl Med Mol Imaging.* 2003; 30: 781-93.
- Korner M, Stockli M, Waser B, Reubi JC. GLP-1 receptor expression in human tumors and human normal tissues: potential for *in vivo* targeting. *J Nucl Med.* 2007; 48: 736-43.
- Tornehave D, Kristensen P, Romer J, Knudsen LB, Heller RS. Expression of the GLP-1 receptor in mouse, rat, and human pancreas. *J Histochem Cytochem.* 2008; 56: 841-51.
- Eng J, Kleinman WA, Singh L, Singh G, Raufman JP. Isolation and characterization of exendin-4, an exendin-3 analogue, from *Heloderma suspectum* venom. Further evidence for an exendin receptor on dispersed acini from guinea pig pancreas. *J Biol Chem.* 1992; 267: 7402-5.
- Goke R, Fehmann HC, Linn T, Schmidt H, Krause M, Eng J, et al. Exendin-4 is a high potency agonist and truncated exendin-(9-39)-amide an antagonist at the glucagon-like peptide 1-(7-36)-amide receptor of insulin-secreting beta-cells. *J Biol Chem.* 1993; 268: 19650-5.
- Fani M, Maecke H R, Okarvi SM. Radiolabeled peptides: valuable tools for the detection and treatment of cancer. *Theranostics.* 2012; 2: 481-501.
- Wild D, Behe M, Wicki A, Storch D, Waser B, Gotthardt M, et al. [Lys<sup>60</sup>(Ahx-DTPA- $^{111}\text{In}$ )NH<sub>2</sub>]exendin-4, a very promising ligand for glucagon-like peptide-1 (GLP-1) receptor targeting. *J Nucl Med.* 2006; 47: 2025-33.
- Christ E, Wild D, Forrer F, Brandle M, Sahli R, Clerici T, et al. Glucagon-like peptide-1 receptor imaging for localization of insulinomas. *J Clin Endocrinol Metab.* 2009; 94: 4398-405.
- Gotthardt M, Lalyko G, van Eerd-Vismale J, Keil B, Schurrat T, Hower M, et al. A new technique for *in vivo* imaging of specific GLP-1 binding sites: first results in small rodents. *Regul Pept.* 2006; 137: 162-7.
- Mukai E, Toyoda K, Kimura H, Kawashima H, Fujimoto H, Ueda M, et al. GLP-1 receptor antagonist as a potential probe for pancreatic beta-cell imaging. *Biochem Biophys Res Commun.* 2009; 389: 523-6.
- Wild D, Wicki A, Mansi R, Behe M, Keil B, Bernhardt P, et al. Exendin-4-based radiopharmaceuticals for glucagonlike peptide-1 receptor PET/CT and SPECT/CT. *J Nucl Med.* 2010; 51: 1059-67.
- Brom M, Oyen WJ, Joosten L, Gotthardt M, Boerman OC.  $^{68}\text{Ga}$ -labelled exendin-3, a new agent for the detection of insulinomas with PET. *Eur J Nucl Med Mol Imaging.* 2010; 37: 1345-55.
- Selvaraju RK, Velikyan I, Johansson L, Wu Z, Todorov I, Shively J, et al. *In Vivo* Imaging of the Glucagonlike Peptide 1 Receptor in the Pancreas with  $^{68}\text{Ga}$ -Labeled DO3A-Exendin-4. *J Nucl Med.* 2013; 54:1458-63.
- Wu Z, Todorov I, Li L, Bading JR, Li Z, Nair I, et al. *In vivo* imaging of transplanted islets with  $^{64}\text{Cu}$ -DO3A-VS-Cys<sup>40</sup>-Exendin-4 by targeting GLP-1 receptor. *Bioconjug Chem.* 2011; 22: 1587-94.
- Connolly BM, Vanko A, McQuade P, Guenther I, Meng X, Rubins D, et al. *Ex vivo* imaging of pancreatic beta cells using a radiolabeled GLP-1 receptor agonist. *Mol Imaging Biol.* 2012; 14: 79-87.
- Kiesewetter DO, Guo N, Guo J, et al. Evaluation of an [ $^{18}\text{F}$ ]AIF-NOTA analog of Exendin-4 for imaging of GLP-1 receptor in insulinoma. *Theranostics.* 2012; 2: 999-1009.
- Kiesewetter DO, Gao H, Ma Y, Niu G, Quan Q, Guo N, et al.  $^{18}\text{F}$ -radiolabeled analogs of exendin-4 for PET imaging of GLP-1 in insulinoma. *Eur J Nucl Med Mol Imaging.* 2012; 39: 463-73.
- Yue X, Kiesewetter DO, Guo J, Sun Z, Zhang X, Zhu L, et al. Development of a new thiol site-specific prosthetic group and its conjugation with [Cys<sup>40</sup>]-exendin-4 for *in vivo* targeting of insulinomas. *Bioconjugate Chem.* 2013; 24:1191-200.
- Wu Z, Liu S, Hassink M, Nair I, Park R, Li L, et al. Development and evaluation of  $^{18}\text{F}$ -TTCO-Cys<sup>40</sup>-Exendin-4: a PET probe for imaging transplanted islets. *J Nucl Med.* 2013; 54: 244-51.
- Wu Z, Li ZB, Cai W, He L, Chin FT, Li F, et al.  $^{18}\text{F}$ -labeled mini-PEG spaced RGD dimer ( $^{18}\text{F}$ -FPRGD2): synthesis and microPET imaging of  $\alpha_5\beta_1$  integrin expression. *Eur J Nucl Med Mol Imaging.* 2007; 34: 1823-31.
- Mammen M, Choi S, Whitesides GM. Polyvalent interactions in biological systems: Implications for design and use of multivalent ligands and inhibitors. *Angew Chem Int Ed.* 1998; 37: 2754-94.
- Cai H, Li Z, Huang CW, Park R, Shahinian AH, Conti PS. An improved synthesis and biological evaluation of a new cage-like bifunctional chelator, 4-((8-amino-3,6,10,13,16,19-hexaazabicyclo[6.6.6]icosane-1-ylamino)methyl)benzoic acid, for  $^{64}\text{Cu}$  radiopharmaceuticals. *Nucl Med Biol.* 2010; 37: 57-65.
- Li Z, Jin Q, Huang C, Dasa S, Chen L, Yap LP, et al. Trackable and Targeted Phage as Positron Emission Tomography (PET) Agent for Cancer Imaging. *Theranostics.* 2011; 1: 371-80.
- Liu S, Li D, Huang CW, Yap LP, Park R, Shan H, et al. The efficient synthesis and biological evaluation of novel bi-functionalized sarcophagine for  $^{64}\text{Cu}$  radiopharmaceuticals. *Theranostics.* 2012; 2: 589-96.
- Liu S, Li D, Huang CW, Yap LP, Park R, Shan H, et al. Efficient Construction of PET/Fluorescence probe based on sarcophagine cage: An opportunity to integrate diagnosis with treatment. *Mol Imaging Biol.* 2012; 14: 718-24.
- Gallwitz B, Witt M, Folsch UR, Creutzfeldt W, Schmidt WE. Binding specificity and signal transduction of receptors for glucagon-like peptide-1(7-36)amide and gastric inhibitory polypeptide on RINm5F insulinoma cells. *J Mol Endocrinol.* 1993; 10: 259-68.
- Omori K, Valiente L, Orr C, Rawson J, Ferreri K, Todorov I, et al. Improvement of human islet cryopreservation by a p38 MAPK inhibitor. *Am J Transplant.* 2007; 7: 1224-32.
- Todorov I, Nair I, Avakian-Mansoorian A, Rawson J, Omori K, Ito T, et al. Quantitative assessment of beta-cell apoptosis and cell composition of isolated, undisturbed human islets by laser scanning cytometry. *Transplantation.* 2010; 90: 836-42.
- Kim TH, Jiang HH, Lee S, Youn YS, Park CW, Byun Y, et al. Mono-PEGylated dimeric exendin-4 as high receptor binding and long-acting conjugates for type 2 anti-diabetes therapeutics. *Bioconjug Chem.* 2012; 22: 625-32.
- Kumar R, Dhanpathi H, Basu S, Rubello D, Fanti S, Alavi A. Oncologic PET tracers beyond [ $^{18}\text{F}$ ]FDG and the novel quantitative approaches in PET imaging. *Q J Nucl Med Mol Imaging.* 2008; 52: 50-65.
- Huang CW, Li Z, Cai H, Chen K, Shahinian T, Conti PS. Design, synthesis and validation of integrin  $\alpha_5\beta_1$ -targeted probe for microPET imaging of prostate cancer. *Eur J Nucl Med Mol Imaging.* 2011; 38: 1313-22.
- van Eerd JE, Vegt E, Wetzels JF, Russel FG, Masereeuw R, Corstens FH, et al. Gelatin-based plasma expander effectively reduces renal uptake of  $^{111}\text{In}$ -octreotide in mice and rats. *J Nucl Med.* 2006; 47: 528-33.
- Chen X, Hou Y, Tohme M, Park R, Khankaldyyan V, Gonzales-Gomez I, et al. Pegylated Arg-Gly-Asp peptide:  $^{64}\text{Cu}$  labeling and PET imaging of brain tumor  $\alpha_5\beta_1$ -integrin expression. *J Nucl Med.* 2004; 45: 1776-83.
- Huang CW, Li Z, Conti PS. *In vivo* near-infrared fluorescence imaging of integrin  $\alpha_5\beta_1$  in prostate cancer with cell-penetrating-peptide-conjugated DGEA probe. *J Nucl Med.* 2011; 52: 1979-86.
- Gotthardt M, van Eerd-Vismale J, Oyen WJ, de Jong M, Zhang H, Rolleman E, et al. Indication for different mechanisms of kidney uptake of radiolabeled peptides. *J Nucl Med.* 2007; 48: 596-601.